

What is the Halo Mass Function in a Fuzzy Dark Matter Cosmology?

Mihir Kulkarni,^{1*} Jeremiah P. Ostriker,^{1†}

¹*Columbia University, Department of Astronomy, New York, NY 10025, U.S.A.*

Accepted XXX. Received YYY; in original form ZZZ

ABSTRACT

Fuzzy dark matter (FDM) or wave dark matter is an alternative theory designed to solve the small-scale problems faced by the standard cold dark matter proposal for the primary material component of the universe. It is made up of ultra-light axions having mass $\sim 10^{-22}$ eV that typically have de Broglie wavelength of several kpc, alleviating some of the apparent small-scale discrepancies faced by the standard Λ CDM paradigm. In this paper, we calculate the halo mass function for the fuzzy dark matter using a sharp-k window function and compare it with one calculated using numerical simulations, finding the peak mass at roughly $10^{10} M_{\odot}$ for a particle mass of 2×10^{-22} eV. We also constrain the mass of FDM particle to be $\gtrsim 2 \times 10^{-22}$ eV using the observations of high-redshift ($z \sim 10$) lensed galaxies from CLASH survey.

Key words: cosmology: dark matter – cosmology: theory – cosmology: early universe – galaxies: high-redshift

1 INTRODUCTION

The standard model of cosmology (Λ CDM) includes dark energy in the form of a cosmological constant and ‘cold’ dark matter. This model has been immensely successful at explaining the large-scale structure of the universe, the statistics of the cosmic microwave background, and cluster abundances (Bennett et al. 2013). However, recent observations have pointed out drawbacks of Λ CDM at small scales. A serious concern is the ‘missing satellite problem’ (Klypin et al. 1999). The number of satellite galaxies predicted for a Milky-way mass galaxy is greater than what we observe by an order of magnitude. This issue is sharpened by the ‘too big to fail’ problem of galaxy formation that claims some of the predicted satellites are so massive that it is impossible for them to not have any stars (Boylan-Kolchin et al. 2011). Λ CDM also predicts a cusp in the center of the density profile of dark matter halos (Navarro et al. 1997), whereas recent observations of dwarf galaxies suggest a flat core (Burkert 1995; Goerdt et al. 2006), although, it is important to note that this issue is not yet settled. In addition, the predicted dynamical friction faced by globular clusters in dwarf spheroidal galaxies is so high that the globular clusters should have spiraled and merged to the center, well before we observe them (Tremaine 1976).

There are typically two types of suggested solutions to these problems. The first attributes these inconsistencies to baryonic physics which is not yet very well understood. For example, the density profile of halos can be flattened to form a core when supernovae and black hole feedback redistributes matter in the galaxy (Navarro et al. 1996). The missing satellite problem could be a result of baryonic physics halting the

formation of galaxies or their destruction by mergers and tidal stripping.

The other set of solutions focus on the nature of dark matter, such as warm dark matter (WDM) and fuzzy dark matter (FDM). These models suppress the small-scale structure of dark matter that results in a cut-off at the lower end of halo mass function. Warm dark matter, which is made up of less massive (\sim keV) particles, remains relativistic for a longer time than CDM. Its thermal velocity wipes out perturbations at small scales (free streaming). It has been pointed out that warm dark matter undergoes a ‘Catch-22’ problem satisfying constraints simultaneously from Lyman- α forests and having large enough cores in dwarf galaxies (Macciò et al. 2012). Macciò et al. (2012) argue that having large enough cores (~ 1 kpc) in dwarf galaxies requires WDM mass to be around 0.1 keV, which prevents the formation of the dwarf galaxies in the first place.

Fuzzy dark matter which is made up of ultra-light axions with masses $\sim 10^{-22}$ eV is another theory of dark matter to solve the small-scale problems (Khlopov et al. 1985; Hu et al. 2000). See Hui et al. (2017) for a detailed review. Their extremely low mass makes their de Broglie wavelengths typically of the order of kpc. This results in a cut-off at small-scales in the power spectrum. The fuzzy dark matter has finite quantum pressure and hence a non-zero effective sound speed given as:

$$c_{s,eff}^2 \approx k^2 / 4a^2 m_a^2, \quad (1)$$

where k is the comoving wave number, a is the scale factor and m_a is the mass of axion. Thus the growth of overdensity is governed by the equation

$$\delta_k + 2H\delta_k + \left(\frac{c_{s,eff}^2 k^2}{a^2} - 4\pi G\rho \right) \delta_k = 0. \quad (2)$$

The solution to Eq. 2 describes the linear growth of perturba-

* E-mail: mihir@astro.columbia.edu

† E-mail: jpo@astro.columbia.edu

tions with sound speed from Eq. 1. For fuzzy dark matter, the perturbations are growing if $(c_{s,eff}^2 k^2 / a^2 < 4\pi G\rho)$. The scale at which two terms are equal is called the Jeans scale,

$$k_J = (16\pi G\rho a^4 m_a^2)^{1/4} = (16\pi G\rho_0 a m_a^2)^{1/4} \quad (3)$$

(Hu et al. 2000). Here, ρ is the background matter density corresponding to a scale factor a and ρ_0 is the background matter density at $z = 0$. The Jeans scale can also be re-written as

$$k_J = 66.5 a^{1/4} \left(\frac{\Omega_a h^2}{0.12} \right)^{1/4} \left(\frac{m}{10^{-22} \text{eV}} \right)^{1/2}, \quad (4)$$

as given by Marsh (2016). Here Ω_a is the ratio of the average axion matter energy density to the critical density and h is defined using $H_0 = 100 h \text{km/s/Mpc}$. A corresponding Jeans mass can be defined as:

$$M_J = \frac{4\pi}{3} \rho_0 \left(\frac{\pi}{k_J} \right)^3 \propto a^{-3/4} m_a^{-3/2}. \quad (5)$$

The Jeans mass at $z = 0$ is $\sim 2 \times 10^7 M_\odot$. Perturbations corresponding to scales slightly larger than the Jeans scale at $z = 0$ are growing in time, however their amplitudes are highly suppressed, as they are smaller than the Jeans scale at some earlier time. An important scale that determines the relative suppression of amplitudes is the Jeans scale at matter-radiation equality, $k_{Jeq} = 9(m_a/10^{-22} \text{eV})^{1/2} \text{Mpc}^{-1}$. The power spectrum for fuzzy dark matter is calculated using a redshift independent transfer function from Hu et al. (2000);

$$P_{FDM}(k, z) = T_F^2(k) P_{CDM}(k, z), \quad T_F(k) = \frac{\cos x^3}{1 + x^8}, \quad (6)$$

where $x = 1.61(m_a/10^{-22} \text{eV})^{1/18} k/k_{Jeq}$. This transfer function is determined by the Jeans scale at matter-radiation equality. As the Jeans length decreases with time, the perturbations at smaller scales continue to grow with time. With the assumption of the redshift independence of transfer function, we assume that the perturbations on all scales continue to grow in time as $\delta \propto D_+$, slightly overestimating the small scale structure.

The transfer function in Eq. 6 is for matter-radiation equality, as it depends on the Jeans scale at that epoch. If we take the initial power spectrum at matter-radiation equality and evolve it numerically using Eq. 2 to $z = 0$, the shape of the power spectrum remains largely unchanged because the scales smaller than the Jeans scale at matter-radiation equality will still be highly suppressed, even if they start growing at a later epoch. This confirms the redshift independence of the transfer function.

In this paper, we calculate the halo mass function using an extended Press-Schechter formalism (Press & Schechter 1974; Bond et al. 1991). We first summarize the previous calculations of the halo mass function by Marsh & Silk (2014); Bozek et al. (2015); Du et al. (2017) that use a spherical top hat window function and a mass dependent critical density. We then point out inconsistencies in their methods and argue why a sharp-k window function works better. We compare our calculations with the halo mass function calculated using collision-less numerical simulations based on the FDM initial power spectrum (Schive et al. 2016).

Early galaxy formation can be used to constrain the properties of FDM, since the short wavelength cutoff in FDM greatly delays galaxy formation at high redshift. Thus, we

also use observations of high redshift ($z \sim 10$) lensed galaxies from CLASH survey to constrain the mass of fuzzy dark matter, following a procedure similar to one used by Pacucci et al. (2013) to constrain warm dark matter.

We use cosmological parameters consistent with WMAP9 data (Hinshaw et al. 2013) ($\Omega_{m0} = 0.284$, $\Omega_\Lambda = 0.716$, $h = 0.696$) so as to be able to compare our results with Schive et al. (2016).

2 CALCULATIONS OF HALO MASS FUNCTION

2.1 Summary of previous calculations

Extended Press-Schechter formalism is widely used for calculating halo mass function for dark matter using the linear power spectrum (Press & Schechter 1974; Bond et al. 1991; Sheth & Tormen 2002).

Variance of perturbation amplitudes in real space smoothed over a scale R is defined as follows:

$$S(R) = \sigma^2(R) = \int_0^\infty \frac{k^2 dk}{2\pi^2} P(k) W^2(kR). \quad (7)$$

A spherical top hat window function is typically used, defined as

$$W_{TH}(kR) = \frac{3(\sin(kR) - kR \cos(kR))}{(kR)^3}. \quad (8)$$

We calculate the trajectory δ_S for a point in space by starting with a large sphere of radius R and decreasing the radius, and calculating the smoothed density contrast for each R . Use of a sharp-k window function makes increments in δ_S independent of previous steps, as $\delta(k)$ are independent Gaussian processes for different k . This use of the sharp-k window function makes this problem analytically solvable. The Press-Schechter (PS) ansatz (Press & Schechter 1974) equates mass element fraction with $\delta_S > \delta_c$ with the mass fraction at time that resides in halos of mass $> M$. Bond et al. (1991) removed cloud-in-cloud inconsistency in PS ansatz by equating the fraction of trajectories with first upcrossing $\delta_S = \delta_c$ at $S > S_1 = \sigma^2(M)$ with the fraction that resides in halos of mass $M < M_1$ (extended Press Schechter formalism).

Following a few steps, we obtain the halo mass function, which is the comoving number density of halos per logarithmic mass bin, given as

$$\frac{dn}{d \ln M} = -\frac{\rho_0}{M} f(\sigma) \frac{d \ln \sigma}{d \ln M}. \quad (9)$$

$$f_{ST}(\sigma) = A \sqrt{\frac{2a}{\pi}} \left[1 + \left(\frac{\sigma^2}{a\delta_c^2} \right)^p \right] \frac{\delta_c}{\sigma} \exp\left(\frac{a\delta_c^2}{2\sigma^2} \right) \quad (10)$$

is the fitting function for Sheth-Tormen mass function, with $A = 0.3222$, $a = 0.707$ and $p = 0.3$. The critical density $\delta_c = 1.686$ is the density contrast at collapse in linear theory for a spherical collapse model.

The halo mass function calculated using this method matches well with the numerical simulations for CDM. But if we follow the same procedure for the fuzzy dark matter, we do not obtain a cut-off in the halo mass function as expected. Figure 1 shows the halo mass functions for CDM and FDM calculated using a top-hat window function and a constant critical density. This produces halos of masses smaller than the Jeans mass for FDM, which is unphysical. The main

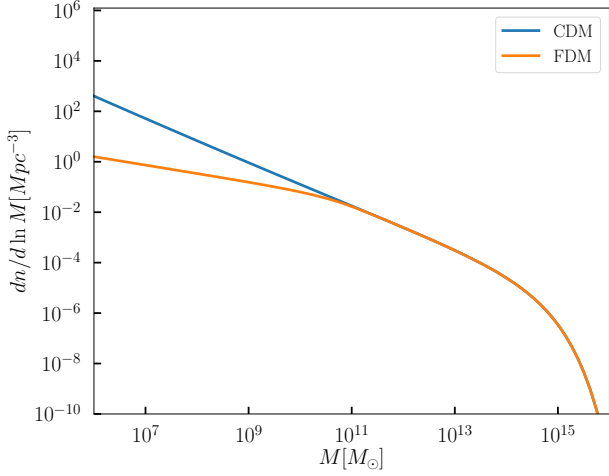


Figure 1. Halo mass functions for CDM and FDM calculated with the extended Press-Schechter formalism using a top hat window function and a constant critical density for $z = 0$. We can see that the halo mass function for FDM does not have a cut-off here as expected.

reason for this is that the top hat window collects the highest contribution from very large scales (small- k modes). For CDM, the dimensionless power spectrum $\Delta_k^2 = k^3 P(k)/(2\pi^2)$ increases for increasing k and hence the spherical top hat window reflects contributions from the scales of interest. FDM has a cut-off in the power spectrum and hence, while calculating $\sigma(R)$ for small R , the major contribution still comes from the large scales in the power spectrum, not reflecting power spectrum amplitudes at corresponding scales.

This can be understood analytically as follows:

$$\frac{d\sigma^2(R)}{dR} = \int_0^\infty \frac{k^2 dk}{2\pi^2} P(k) \frac{dW_R^2(k)}{dR}, \quad (11)$$

$$W_{TH}(x) = \frac{3}{x^4} ((x^2 - 3) \sin x + 3x \cos x) = \frac{3}{x} \left(\frac{\sin(x)}{x} - W_{TH}(x) \right), \quad (12)$$

$$\frac{dW_{TH}^2}{dR} = \frac{6W_{TH}(kR)}{R} \left(\frac{\sin(kR)}{kR} - W_{TH}(kR) \right), \quad (13)$$

which in the limit of $R \rightarrow 0$ becomes $\propto -R$. This tells us that the derivative of the window function has a tail stretching over small R . Plugging this into Eq. 11 gives that $\frac{d\sigma^2(R)}{dR} \propto R$ for small R . So,

$$\frac{dn}{d \ln M} = -\frac{\rho_0}{M} f(\sigma) \frac{d \ln \sigma}{d \ln M} \propto -\frac{1}{M} \frac{d \ln \sigma}{d \ln M} \propto -\frac{1}{M} R \frac{dW_{TH}^2}{dR} \propto \frac{1}{R}, \quad (14)$$

which means that the halo mass function diverges as $M \rightarrow 0$ and does not give a cut-off as required.

Solutions by Marsh & Silk (2014); Bozek et al. (2015); Du et al. (2017) involve using a mass dependent critical density to suppress the halo mass function at lower masses. The new critical density is defined as

$$\delta_c^{fdm}(M, z) = G(k, z) \delta_c^{cdm}(z), \quad (15)$$

where $G(k, z)$ is given as

$$G(k, z) = \frac{\delta_{cdm}(k, z) \delta_{cdm}(k_0, z_h)}{\delta_{cdm}(k, z_h) \delta_{cdm}(k_0, z)} \frac{\delta_{fdm}(k, z) \delta_{fdm}(k_0, z_h)}{\delta_{fdm}(k, z_h) \delta_{fdm}(k_0, z)}, \quad (16)$$

where where $k_0 = 0.002 \text{ h/Mpc}$ is a pivot scale, and z_h is chosen to be large enough so that at the relevant redshift the shape of CDM power spectrum has frozen in, selected to be 300 by Du et al. (2017). The argument used for using this critical density is as follows: For CDM, we can take $\delta_c = 1.686$ to be a constant and take $\sigma(R, z) \propto D_+(z)$, or we can make δ_c redshift dependent as $\delta_c \propto 1/D_+(z)$ and $\sigma(R)$ to be redshift independent. The growth rate for CDM is scale independent and hence we can use a scale-independent critical density. On the other hand, FDM growth is scale-dependent and hence one should use a critical density which is higher for lower masses.

Marsh & Silk (2014) and Bozek et al. (2015) use this mass dependent critical density and fitting function $f(\sigma)$ given by Sheth & Tormen (2002). Du et al. (2017) use the same mass dependent critical density, but argue that the same fitting function cannot be used. The fitting function $f(\sigma)$ and the critical density (barrier) are related to each other in the Press-Schechter formalism as:

$$\int_0^S f(S') dS' + \int_{-\infty}^{B(S)} P(\delta, S) d\delta = 1, \quad (17)$$

where $S = \sigma^2$, $B(S)$ is the mass dependent barrier and $P(\delta, S)$ is the probability for a trajectory to lie between δ and $\delta + d\delta$ for variance S . Du et al. (2017) numerically calculate $f(\sigma)$ for the mass dependent critical density. This changes few properties of the halo mass function.

Both calculations by Marsh & Silk (2014); Bozek et al. (2015) and Du et al. (2017) give sharp cut-offs in the halo mass function and the cut-offs increase as we go to higher redshifts. The cut-off for Marsh & Silk (2014) and Bozek et al. (2015) is $\sim 2 \times 10^8 M_\odot$ for $m_a = 10^{-22} \text{ eV}$ at $z = 0$. Whereas one calculated by Du et al. (2017) is about four times higher. For redshift 14, Marsh & Silk (2014) and Bozek et al. (2015) obtain a cut-off at $2 \times 10^9 M_\odot$, whereas Du et al. (2017) have it to be $3 \times 10^9 M_\odot$.

Du et al. (2017) calculate the cut-offs to be higher than those calculated by Marsh & Silk (2014) or Bozek et al. (2015). It is also worth noting that the cut-off mass changes less strongly with redshift in Du et al. (2017).

2.2 Shortcomings of previous calculations

The argument for a mass dependent critical density is based on the fact that $\sigma(R, z) \propto D_+(z)$ or inversely for δ_c for CDM and that this growth factor $D_+(z)$ should be replaced with $D_+(k, z)$ for FDM. Let us take a closer look at this argument.

For fuzzy dark matter, $\sigma(R)$ becomes nearly constant for R smaller than the cut-off scale in the power spectrum. The shape of $\sigma(R)$ is very weakly dependent on the shape of the power spectrum for scales smaller than the cut-off scale, as the spherical top hat window draws contributions mainly from large scales.

$$\sigma(R) \approx \sigma(R_0) \quad \text{for } R < R_0 \quad (18)$$

Hence, the redshift dependence of $\sigma(R)$ can be given as

$$\sigma(R, z) = \begin{cases} \frac{D_+(R, z)}{D_+(R, z_0)} \sigma(R, z_0) & \text{for } R > R_0, \\ \frac{D_+(R_0, z)}{D_+(R_0, z_0)} \sigma(R, z_0) & \text{for } R < R_0. \end{cases} \quad (19)$$

$$\therefore \sigma(R, z) = \frac{D_+(z)}{D_+(z_0)} \sigma(R, z_0). \quad (20)$$

Here, R_0 corresponds to the scale where the FDM power spectrum starts to differ from CDM (approximately the Jeans scale at the matter-radiation equality). The scales larger than or equal to R_0 grow the same as CDM, which concludes that $\sigma(R)$ for FDM grows in a fashion similar to CDM with redshift. Hence, the critical density also cannot be dependent on the scale through the FDM growth rate.

It is also interesting to note that the redshift dependence in the halo mass functions calculated by [Marsh & Silk \(2014\)](#); [Du et al. \(2017\)](#) comes mainly from the redshift dependence of the Jeans scale. The shape of the power spectrum and $\sigma(R)$ does not change with significantly the redshift, as the transfer function is nearly redshift independent ([Hu et al. 2000](#)). However, the shape of the critical density barrier changes with redshift, as it is based on which scales are growing and which are not. In their Figure 3, [Du et al. \(2017\)](#) show the halo mass function calculated using a redshift dependent transfer function, whereas in Figure 5, they use the transfer function given by [Hu et al. \(2000\)](#). For both the cases, for $m_a = 10^{-22}$ eV at $z = 0$, they find a cutoff in the halo mass function at $6 \times 10^8 h^{-1} M_\odot$. Therefore, we conclude that the redshift dependence in the cutoff of the halo mass function in [Du et al. \(2017\)](#) arises primarily not from the redshift evolution of the transfer function, but from the redshift evolution of the Jeans mass and the mass-dependent barrier.

In recent years, there have been many simulations that solve the Schrödinger-Poisson equations for accurately evolving FDM ([Schive et al. 2014a,b](#); [Mocz et al. 2017](#); [Li et al. 2019](#)). Although they accurately evolve fuzzy dark matter and reproduce the soliton profiles in the halos, they do not have a sufficient number of halos to calculate the halo mass function because of their small box sizes. A number of works ([Schive et al. 2016](#); [Sarkar et al. 2016](#); [Zhang et al. 2018](#); [Nori et al. 2019](#)) have run collision-less N-body simulations with the initial power spectrum of FDM. These numerical simulations predict many lower mass halos too. [Schive et al. \(2016\)](#) mark and delete those ‘spurious’ halos and calculate the halo mass function for ‘genuine’ halos. Hence, we use the halo mass function estimated in [Schive et al. \(2016\)](#) to compare with our results.

[Du et al. \(2017\)](#) return their halo mass function for $m_a = 10^{-22}$ eV, whereas [Schive et al. \(2016\)](#) return their results for $m_a = 0.8, 1.6, 3 \times 10^{-22}$ eV. We compare the results for $m_a = 0.8 \times 10^{-22}$ eV with results from [Du et al. \(2017\)](#). [Du et al. \(2017\)](#) calculate the cut-off mass for redshift 4 to be $\sim 1.5 \times 10^9 M_\odot$. This cut-off will be slightly higher for $m_a = 0.8 \times 10^{-22}$ eV. [Schive et al. \(2016\)](#) have halos as small as $4 \times 10^8 M_\odot$ which is clearly smaller than the predicted cut-off from [Du et al. \(2017\)](#).

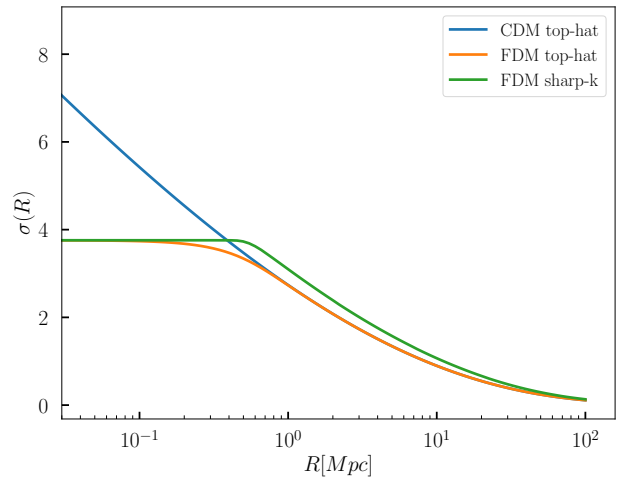


Figure 2. $\sigma(R)$ using top hat window function for CDM and FDM as well as $\sigma(R)$ for FDM using sharp-k window function.

2.3 HMF using a sharp-k window function

Instead of using the spherical top hat function and a mass dependent critical density, we use a sharp-k window function and a constant critical density in this work. This approach has been previously used for the warm dark matter ([Benson et al. 2013](#); [Schneider et al. 2013](#)) and was also used for the fuzzy dark matter recently by [Linares Cedeño et al. \(2021\)](#).

$$W_R(k) = \begin{cases} 1 & \text{for } k \leq k_0 \\ 0 & \text{for } k > k_0 \end{cases} \quad (21)$$

A drawback of the sharp-k window is that the enclosed mass is not clearly defined in it. It has contributions from all scales in real space, making it difficult to assign a mass M for a given k_0 . A similar problem is faced by a Gaussian window function, but it can be assigned a mass based on its integration in real space. The integration of the sharp-k window function in real space diverges ([Maggiore & Riotto 2010](#)). Previous works ([Benson et al. 2013](#); [Schneider et al. 2013](#)) using a sharp-k window with warm dark matter use $k_0 = \alpha/R$ keeping a free parameter to be fit by the numerical simulations. Following [Benson et al. \(2013\)](#), we use $\alpha = 2.5$, which is also close to the value of 2.42 suggested by [Lacey & Cole \(1994\)](#) using an approximate integral. We also need to rescale the critical density, as $\sigma(R)$ with sharp-k window is higher than that of top hat window for higher masses (see Figure 2). We rescale δ_c by multiplying it with 1.195. This is also to ensure that the halo mass function matches with CDM at higher masses.

This halo mass function does not give a sharp cut-off like [Marsh & Silk \(2014\)](#); [Bozek et al. \(2015\)](#); [Du et al. \(2017\)](#). Figure 3 shows the halo mass function for different FDM mass. The cut-off does not depend on redshift as strongly as previous works. Figure 4 shows FDM halo mass functions for different redshifts for $m_a = 2 \times 10^{-22}$ eV.

The calculated halo mass function is shown in figure 5 along with the halo mass function calculated by [Schive et al. \(2016\)](#) for $m_a = 3.2 \times 10^{-22}$ eV and $m_a = 1.6 \times 10^{-22}$ eV at $z = 4$. [Schive](#)

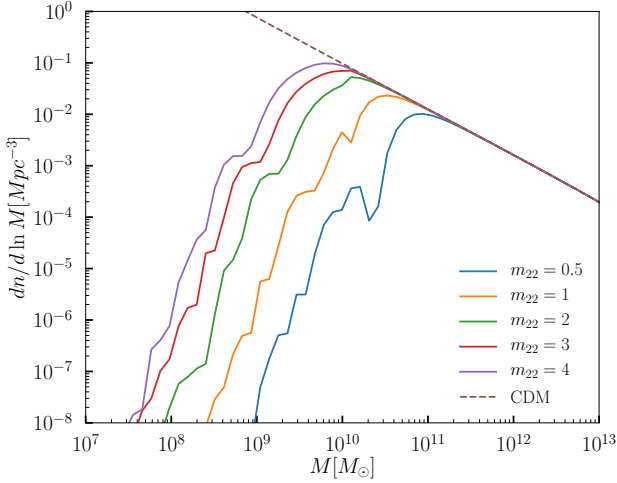


Figure 3. Halo mass functions calculated using the sharp-k window function for m_a of 0.5, 1, 2, 3, 4 $\times 10^{-22}$ eV for FDM and for CDM at $z = 0$.

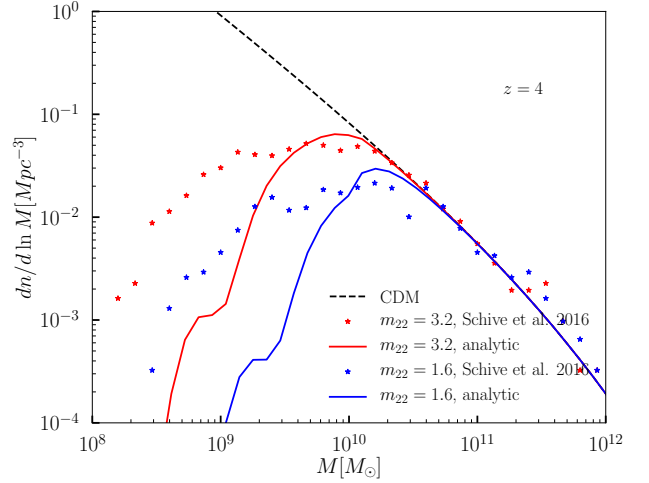


Figure 5. Halo mass functions for $m_a = 1.6 \times 10^{-22}$ eV and $m_a = 3.2 \times 10^{-22}$ eV at redshift 4 from analytic calculations using a sharp-k window function, and from simulations by Schive et al. (2016).

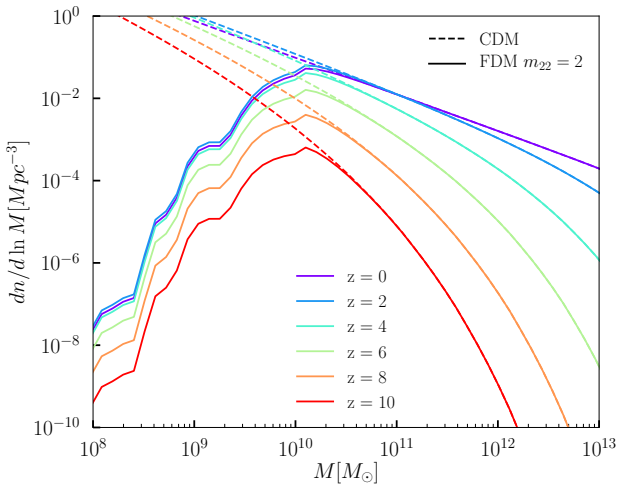


Figure 4. Halo mass functions calculated using the sharp-k window function for various redshifts for $m_a = 2 \times 10^{-22}$ eV. The halo mass function is smoothed for masses lower than $5 \times 10^{10} M_\odot$.

et al. (2016) use collision-less dark matter simulation with an initial power spectrum for fuzzy dark matter.

We note that the analytical halo mass function we have derived predicts a lower number of halos compared to the numerical simulations at low masses as shown in Figure 5. There could be two possible reasons for this:

- In their simulation, Schive et al. (2016) find many low mass halos. They flag “spurious” halos and remove them from their calculations. It is possible that a sufficient number of halos have not been removed. A full non-linear simulation solving the Schrödinger-Poisson equations is required to make an accurate comparison.

- Fuzzy dark matter power spectrum falls much more rapidly as compared to the warm dark matter. Hence, halo formation from non-linear effects such as fragmentation of larger structures could be significant, and this is not considered in this calculation. This could increase the number of halos at low masses. This needs further investigation.

We agree with the shortcomings of our model to calculate the halo mass function using a sharp-k window function, particularly below the turnover halo mass scale. It needs a further investigation of the non-linear structure formation and an accurate estimation of the halo mass function from the simulations of fuzzy dark matter that use Schrödinger-Poisson equations. Recent work by May & Springel (2021) suggests that the turnover in the halo mass function at the low mass end may not be as steep as we find here and finds a higher number of low mass halos. For this exercise however, we will use the analytical halo mass function that we have calculated to constrain the mass of FDM.

3 LIMITS ON THE FDM MASS

The fuzzy dark matter paradigm has only one parameter m_a . The FDM particle is lighter than 10^{-18} eV and massive than 10^{-33} eV (Marsh 2016). The mass can further be constrained by various astrophysical processes including the following. Schive et al. (2016); Bozek et al. (2015) use galaxy UV luminosity function and Schive et al. (2016) constrain it to be $> 1.2 \times 10^{-22}$ eV. Sarkar et al. (2016) found $m_a > 10^{-23}$ eV using damped Lyman- α observations and simulations. Calabrese & Spergel (2016) have used the cored density profile from Schive et al. (2014b) and observations of newly discovered ultra faint dSphs and estimated m_a to be $3.7 - 5.6 \times 10^{-22}$ eV. Amorisco & Loeb (2018) constrain $m_a > 1.5 \times 10^{-22}$ eV based on the dynamics of stellar streams in the Milky Way. Observations of high-resolution Lyman- α spectra were used to constrain the axion mass to be more than 10^{-21} eV (Armengaud et al. 2017;

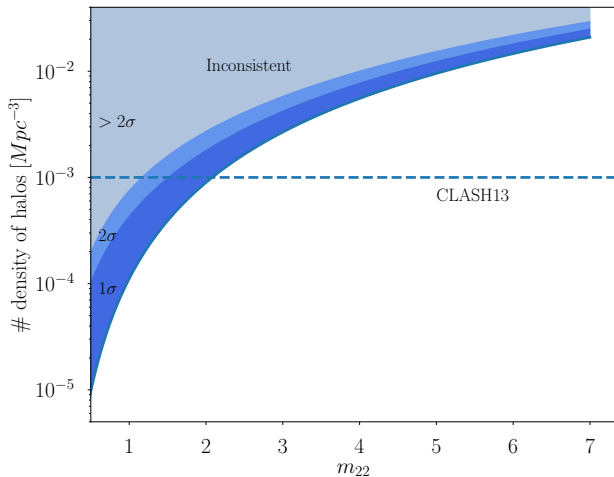


Figure 6. Integrated number density of halos as a function of axion mass at $z = 10$. The horizontal line at 10^{-3} Mpc^{-3} denotes the number density from observations. The errors are Poisson errors.

Iršič et al. 2017; Kobayashi et al. 2017), although further work needs to be done to understand the effects of baryonic physics better. In particular, late reionization can leave a patchy distribution of neutral hydrogen that can be falsely interpreted as due to gravitational fluctuations.

In this work, we constrain the mass of axions using observations of high-redshift lensed galaxies following a method used by Pacucci et al. (2013) to constrain the warm dark matter.

Cluster Lensing And Supernova survey with Hubble (CLASH) is a survey using the Hubble telescope. Zheng et al. (2012) report the observation of a galaxy at redshift 9.6 with a magnification of 15 (MACS 1149-JD). Coe et al. (2013) report the observation of another galaxy at redshift ~ 10.8 with a magnification of 8 (MACS0647-JD). Coe et al. (2013) estimate intrinsic (unlensed) magnitude of MACS0647-JD to be 28.2 in F160W band and calculate the rest frame UV luminosity to be $L_{UV} \sim 2.8 \times 10^{28} \text{ erg s}^{-1} \text{ Hz}^{-1}$. They conclude that the stellar mass of galaxy is most likely $10^8 - 10^9 M_{\odot}$ and expect the dark halo mass to be $\sim 10^{10} M_{\odot}$. We do not use the mass of the galaxy for constraining the axion mass. The magnification factor can be used to calculate the effective volume of the galaxies. Existence of galaxies at $z \sim 10$ with their effective volume can be used to constrain the fuzzy dark matter, even without explicit knowledge about masses of the galaxies.

Object ID	μ	V_{eff} (Mpc^3)
MACS1149-JD	15	~ 700
MACS0647-JD	8	~ 2000

$$n(m_a, z) = \int_0^{\infty} \frac{dn}{d \ln M}(M, z, m_a) d \ln M \quad (22)$$

We calculate the halo mass function for the fuzzy dark matter at redshift 10. We integrate the halo mass function to get the integrated number density of halos as a function of axion mass. Since this includes halos of all masses, the number density calculated from observations cannot be higher than this.

If we conservatively use the effective volume for two

galaxies to be 2000 Mpc^3 , that gives $n_{tot} = 2/2000 \text{ Mpc}^{-3} = 10^{-3} \text{ Mpc}^{-3}$. Figure 6 shows a plot of cumulative number density as a function of FDM mass. We calculate Poisson errors on the number of halos in the corresponding volume i.e. 1000 Mpc^3 . The intersection of the integrated number density and horizontal line corresponding to CLASH survey gives a lower limit on the axion mass. With this exercise we calculate to be $m_a > 2 \times 10^{-22} \text{ eV}$. With $2 - \sigma$ error (95% confidence interval), the minimum mass of axion is constrained to be $1.2 \times 10^{-22} \text{ eV}$.

While calculating this constraint, we have not used any astrophysical processes other than the halo mass function. We have integrated over the entire halo mass function. Tighter constraints can be obtained by accurately simulating the stellar properties of first galaxies in FDM, observations of lensed galaxies at higher redshifts and geometries of the effective volume. As the early galaxy formation is significantly delayed in a fuzzy dark matter cosmology, observations of high-redshift galaxies coupled with accurate numerical predictions may be the best way to constrain FDM. The *Roman Space Telescope (WFIRST)* High Latitude Survey is expected to observe many $z \sim 10$ galaxies (Spergel et al. 2013; Waters et al. 2016) which can be studied in detail with the *James Webb Space Telescope (JWST)*. The *JWST* is also expected to measure the faint-end of the UV luminosity function at high-redshift which can also be used to constrain the properties of the fuzzy dark matter (Corasaniti et al. 2017; Ni et al. 2019).

ACKNOWLEDGEMENTS

We thank Zoltán Haiman for suggesting the method to constrain the axion mass; Lam Hui, Hsi-Yu Schive, and Tom Broadhurst for helpful discussions and Hsi-Yu Schive for providing the simulation data.

DATA AVAILABILITY

No new data were generated or analysed in support of this research. Numerical code to calculate the halo mass function will be shared on reasonable request to the corresponding author.

REFERENCES

- Amorisco N. C., Loeb A., 2018, arXiv e-prints, p. [arXiv:1808.00464](https://arxiv.org/abs/1808.00464)
- Armengaud E., Palanque-Delabrouille N., Yèche C., Marsh D. J. E., Baur J., 2017, *MNRAS*, **471**, 4606
- Bennett C. L., et al., 2013, *ApJS*, **208**, 20
- Benson A. J., et al., 2013, *MNRAS*, **428**, 1774
- Bond J. R., Cole S., Efstathiou G., Kaiser N., 1991, *ApJ*, **379**, 440
- Boylan-Kolchin M., Bullock J. S., Kaplinghat M., 2011, *MNRAS*, **415**, L40
- Bozek B., Marsh D. J. E., Silk J., Wyse R. F. G., 2015, *MNRAS*, **450**, 209
- Burkert A., 1995, *ApJ*, **447**, L25
- Calabrese E., Spergel D. N., 2016, *MNRAS*, **460**, 4397
- Coe D., et al., 2013, *ApJ*, **762**, 32
- Corasaniti P. S., Agarwal S., Marsh D. J. E., Das S., 2017, *Phys. Rev. D*, **95**, 083512
- Du X., Behrens C., Niemeyer J. C., 2017, *MNRAS*, **465**, 941

- Goerdt T., Moore B., Read J. I., Stadel J., Zemp M., 2006, *MNRAS*, **368**, 1073
- Hinshaw G., et al., 2013, *ApJS*, **208**, 19
- Hu W., Barkana R., Gruzinov A., 2000, *Physical Review Letters*, **85**, 1158
- Hui L., Ostriker J. P., Tremaine S., Witten E., 2017, *Phys. Rev. D*, **95**, 043541
- Iršič V., Viel M., Haehnelt M. G., Bolton J. S., Becker G. D., 2017, *Phys. Rev. Lett.*, **119**, 031302
- Khlopov M. I., Malomed B. A., Zeldovich I. B., 1985, *MNRAS*, **215**, 575
- Klypin A., Kravtsov A. V., Valenzuela O., Prada F., 1999, *ApJ*, **522**, 82
- Kobayashi T., Murgia R., De Simone A., Iršič V., Viel M., 2017, *Phys. Rev. D*, **96**, 123514
- Lacey C., Cole S., 1994, *MNRAS*, **271**, 676
- Li X., Hui L., Bryan G. L., 2019, *Phys. Rev. D*, **99**, 063509
- Linares Cedeño F. X., González-Morales A. X., Ureña-López L. A., 2021, *J. Cosmology Astropart. Phys.*, **2021**, 051
- Macciò A. V., Paduroiu S., Anderhalden D., Schneider A., Moore B., 2012, *MNRAS*, **424**, 1105
- Maggiore M., Riotto A., 2010, *ApJ*, **711**, 907
- Marsh D. J. E., 2016, *Phys. Rep.*, **643**, 1
- Marsh D. J. E., Silk J., 2014, *MNRAS*, **437**, 2652
- May S., Springel V., 2021, *MNRAS*, **506**, 2603
- Mocz P., Vogelsberger M., Robles V. H., Zavala J., Boylan-Kolchin M., Fialkov A., Hernquist L., 2017, *MNRAS*, **471**, 4559
- Navarro J. F., Eke V. R., Frenk C. S., 1996, *MNRAS*, **283**, L72
- Navarro J. F., Frenk C. S., White S. D. M., 1997, *ApJ*, **490**, 493
- Ni Y., Wang M.-Y., Feng Y., Di Matteo T., 2019, *MNRAS*, **488**, 5551
- Nori M., Murgia R., Iršič V., Baldi M., Viel M., 2019, *MNRAS*, **482**, 3227
- Pacucci F., Mesinger A., Haiman Z., 2013, *MNRAS*, **435**, L53
- Press W. H., Schechter P., 1974, *ApJ*, **187**, 425
- Sarkar A., Mondal R., Das S., Sethi S. K., Bharadwaj S., Marsh D. J. E., 2016, *J. Cosmology Astropart. Phys.*, **4**, 012
- Schive H.-Y., Chiueh T., Broadhurst T., 2014a, *Nature Physics*, **10**, 496
- Schive H.-Y., Liao M.-H., Woo T.-P., Wong S.-K., Chiueh T., Broadhurst T., Hwang W.-Y. P., 2014b, *Physical Review Letters*, **113**, 261302
- Schive H.-Y., Chiueh T., Broadhurst T., Huang K.-W., 2016, *ApJ*, **818**, 89
- Schneider A., Smith R. E., Reed D., 2013, *MNRAS*, **433**, 1573
- Sheth R. K., Tormen G., 2002, *MNRAS*, **329**, 61
- Spergel D., et al., 2013, arXiv e-prints, p. [arXiv:1305.5425](https://arxiv.org/abs/1305.5425)
- Tremaine S. D., 1976, *ApJ*, **203**, 345
- Waters D., Di Matteo T., Feng Y., Wilkins S. M., Croft R. A. C., 2016, *MNRAS*, **463**, 3520
- Zhang J., Kuo J.-L., Liu H., Sming Tsai Y.-L., Cheung K., Chu M.-C., 2018, *ApJ*, **863**, 73
- Zheng W., et al., 2012, *Nature*, **489**, 406

This paper has been typeset from a $\text{\TeX}/\text{\LaTeX}$ file prepared by the author.